The Journal of the Oceanological Society of Korea
Vol. 15, No. 2, p. 112~122, Dec. 1980

# TIDAL COMPUTATIONS FOR INCHON BAY

*Byung Ho Choi*

Korea Ocean Research and Development Institute, KIST

## ABSTRACT

A two-dimensional non-linear tidal model has been established to calculate the $M_2$ tide of Inchon Bay in the west coast of Korea. Cartesian coordinates are used for the derivation of the governing equations and account is taken of extensive drying boundaries (tidal flats) which are exposed at low tides. The tidal amplitudes and phases computed from the model agree well with those known from observation lying within bounds ±5cm in amplitude and ±5° in phase relative to the observed results. The work represents a further stage in the development including extensive sea measurements capable of application in various coastal engineering problems encountered in Inchon Bay area.

## INTRODUCTION

In regions of the world where high tidal ranges are recorded, the high ranges are caused in part by the configurations of the coastline. The construction of a major barrier across a coastal inlet can therefore be expected to affect the tidal regime and, in extreme cases, very significantly change the tidal range where the barrier and coastal structures are designed to construct. Accordingly, it is important that the effects of proposed tidal barriers for various purpose including water storage, land reclamation and tidal power schemes on the tidal regime be assessed.

Numerical finite-difference models, usually formulated on the basis of the vertically integrated or depth-averaged hydrodynamical equations, have been used quite extensively for some years and with considerable success in reproducing tide and storm surges in shallow seas and estuaries. The method of predicting tidal changes by barrier construction via mathematical model studies have been well established (Heaps, 1972; Heaps and Greenberg, 1974). Mathematical model studies which are to assess the effects of tidal barriers constructed along the Inchon Bay area were initiated during 1977 and these studies are being continued at KORDI. The present paper covers the development of two-dimensional non-linear model restricting to Inchon Bay to investigate the $M_2$ tide distribution. Subsequent estimation of barrier effects on $M_2$ tide regime utilising this model was presented previously (Choi, 1978).

In the finite difference grid of the model as shown in Fig. 1, Cartesian coordinates are used for the derivation of the governing equations. An essential requirement for modelling of Inchon Bay area is the proper representation of drying banks, which are exposed as the water level falls on the ebb, and which are re-submerged on the flood as the level rises again. Among a number of difference schemes for shoaling water computations (Rein and Bodine, 1968; Sielecki and Wurtele, 1970; Leendertse and Gritton, 1971; Ramming, 1972; Flather and Heaps, 1975) which simulate drying banks, the scheme used for Morecambe Bay (Flather and Heaps, 1975) was used for the present study.

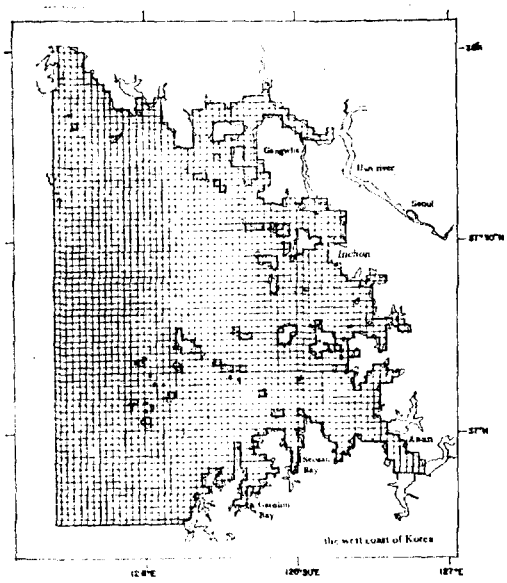


**Fig. 1.** Inchon Bay model finite difference grid

## A tidal model of Inchon Bay

### 1. Basic equations

The equation of continuity and depth-mean motion for co-oscillating tides on a flat rotating sea are (Flather & Heaps, 1975):

$$\frac{\partial \zeta}{\partial t}+\frac{\partial}{\partial x}(Hu)+\frac{\partial}{\partial y}(Hv)=0, \tag{1}$$

$$\frac{\partial u}{\partial t}+u\frac{\partial u}{\partial x}+v\frac{\partial u}{\partial y}-fv+\frac{\kappa u(u^2+v^2)^{\frac{1}{2}}}{H}+g\frac{\partial \zeta}{\partial x}=0, \tag{2}$$

$$\frac{\partial v}{\partial t}+u\frac{\partial v}{\partial x}+v\frac{\partial v}{\partial y}+fu+\frac{\kappa v(u^2+v^2)^{\frac{1}{2}}}{H}+g\frac{\partial \zeta}{\partial y}=0, \tag{3}$$

where the notation is

$x, y$: Cartesian coordinates in the horizontal plane of the undisturbed sea surface

$t$: time

$\zeta$: elevation of the sea surface

$u, v$: components of the depth-mean current in the directions of increasing $x, y$ respectively,

$H$: total depth of water $=h+\zeta$

$h$: undisturbed depth of water

$f$: Coriolis parameter, assumed constant

$\kappa$: coefficient of bottom friction

$g$: acceleration due to the Earth's gravity

The depth-mean currents are defined as:

$$u=\frac{1}{H}\int_{-h}^{\zeta}u'dz,\quad v=\frac{1}{H}\int_{-h}^{\zeta}v'dz \tag{4}$$

where $u', v'$ are components of horizontal current at depth $z$ below the sea surface. In order to obtain the depth-averaged form of advective terms in (2) and (3) it has to be assumed that the currents do not vary significantly in the vertical so that

$$\int_{-h}^{\zeta}u'^2dz=Hu^2,\quad \int_{-h}^{\zeta}u'v'dz=Huv,$$

$$\int_{-h}^{\zeta}v'^2dz=Hv^2.$$

Initial and boundary conditions required for the solution of equation (1) to (3) are as follows:

At $t=0$ : $u(x, y, t)$, $v(x, y, t)$ and $\zeta(x, y, t)$ are specified for all positions at which the equations are to be solved.

At a land boundary: the component of the flow normal to the boundary is permanently zero:

$$u\cos\theta+v\sin\theta=0$$

where $\theta$ is the angle between the normal to the coast directed out of the sea region and the $x$ axis, therefore

$u=0$ is the boundary condition at $y$ directed land boundary

$v=0$ is the boundary condition at $x$ directed land boundary

Along an open boundary, elevation or current is specified as a function of time and posion along the boundary

$$\zeta=\hat{\zeta}(x, y, t)$$

or

$$q_n=\hat{q}_n(x, y, t)$$

where $q_n=u\cos\alpha+v\sin\alpha$ and $\alpha$ denotes the inclination of the outward directed normal to the axis of $x$.

## 2. Numerical scheme

The equations (1) (2) (3) were written into following finite difference form, excluding the advective terms, using a spatial grid notation as shown in Fig. 2.

$$\frac{\zeta_i(t+\Delta t)-\zeta_i(t)}{\Delta t} = -\frac{1}{\Delta s}\{d_i(t)u_i(t)-d_{i-1}(t)u_{i-1}(t) + e_{i-n}(t)v_{i-n}(t)-e_i(t)v_i(t)\}, \tag{5}$$

$$\frac{u_i(t+\Delta t)-u_i(t)}{\Delta t} = fr_i(t)-g\frac{\{\zeta_{i+1}(t+\Delta t)-\zeta_i(t+\Delta t)\}}{\Delta s} - \frac{\kappa u_i(t)\{u_i^2(t)+r_i^2(t)\}^{\frac{1}{2}}}{D_i(t)}, \tag{6}$$

$$\frac{v_i(t+\Delta t)-v_i(t)}{\Delta t} = -fs_i(t+\Delta t)-g\frac{\{\zeta_i(t+\Delta t)-\zeta_{i+n}(t+\Delta t)\}}{\Delta s} - \frac{\kappa v_i(t)\{s_i^2(t)+v_i^2(t)\}^{\frac{1}{2}}}{E_i(t)}, \tag{7}$$

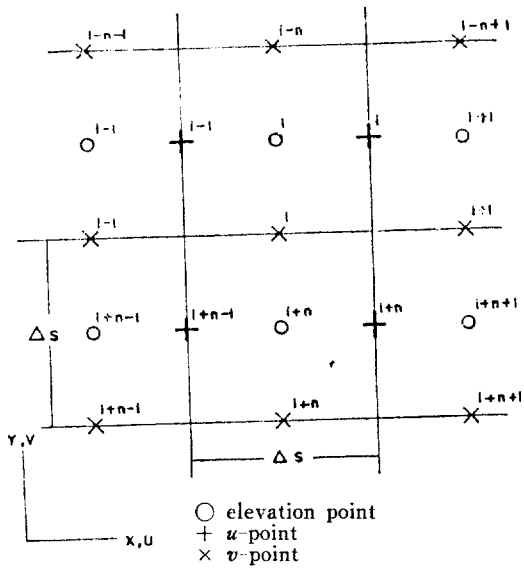


**Fig.** 2. Spatial grid of the model

where $d_i=\frac{1}{2}(h_i+\zeta_i+h_{i+1}+\zeta_{i+1})$,

$e_i=\frac{1}{2}(h_i+\zeta_i+h_{i+n}+\zeta_{i+n})$,

$r_i=\frac{1}{4}(v_{i-n}+v_{i-n+1}+v_i+v_{i+1})$,

$s_i=\frac{1}{4}(u_{i-1}+u_i+u_{i+n-1}+u_{i+n})$,

$D_i=\max(d_i,\ H_0)$, $E_i=\max(e_i,\ H_0)$

$H_0$=postulated minimum depth.

The frictional terms in equations (6) (7) are modified as follows to achieve stability in shallow water area (Flather 1972).

$$\frac{u_i(t+\Delta t)-u_i(t)}{\Delta t} = fr_i(t)-g\frac{\{\zeta_{i+1}(t+\Delta t)-\zeta_i(t+\Delta t)\}}{\Delta s} - \frac{\kappa u_i(t+\Delta t)\{u_i^2(t)+r_i^2(t)\}^{\frac{1}{2}}}{D_i(t)}, \tag{8}$$

$$\frac{v_i(t+\Delta t)-v_i(t)}{\Delta t} = fs_i(t+\Delta t)-g\frac{\{\zeta_i(t+\Delta t)-\zeta_{i+n}(t+\Delta t)\}}{\Delta s} - \frac{\kappa v_i(t+\Delta t)\{s_i^2(t)+v_i^2(t)\}^{\frac{1}{2}}}{E_i(t)}, \tag{9}$$

Hence, we get:

$$u_i(t+\Delta t)=\frac{u_i(t)+f\Delta t r_i(t)-g\{\zeta_{i+1}(t+\Delta t)-\zeta_i(t+\Delta t)\}\Delta t/\Delta s}{1+\kappa\Delta t\{u_i^2(t)+r_i^2(t)\}^{\frac{1}{2}}/D_i(t)}, \tag{10}$$

$$v_i(t+\Delta t)=\frac{v_i(t)-f\Delta t s_i(t+\Delta t)-g\{\zeta_i(t+\Delta t)-\zeta_{i+n}(t+\Delta t)\}\Delta t/\Delta s}{1+\kappa\Delta t\{s_i^2(t)+v_i^2(t)^{\frac{1}{2}}/E_i(t)}, \tag{11}$$

Using the angled-derivative scheme for advective terms which was used successfully by Flather and Heaps (1975) by alternating the direction of scanning the grid and the order of updating $u$ and $v$, the equations of motion (8) and (9) are replaced by:

in an odd timestep: positive scan calculating $u$ first then $v$,

$$\left.\begin{aligned}\frac{\{u_i(t+\Delta t)-u_i(t)\}}{\Delta t} = &-\frac{1}{2\Delta s}\bar{u}_i(t)\{u_{i+1}(t)-u_i(t)+u_i(t+\Delta t)-u_{i-1}(t+\Delta t)\}\\ &-\frac{1}{4\Delta s}[\{v_{i-n}(t)+v_{i-n+1}(t)\}\{u_{i-n}(t+\Delta t)-u_i(t+\Delta t)\}\\ &+\{v_i(t)+v_{i+1}(t)\}\{u_i(t)-u_{i+n}(t)\}]\\ &+fr_i(t)-\kappa u_i(t+\Delta t)\{u_i^2(t)+r_i^2(t)\}^{\frac{1}{2}}/D_i(t)-g\{\zeta_{i+1}(t+\Delta t)-\zeta_i(t+\Delta t)\}/\Delta s\end{aligned}\right\} \tag{12}$$

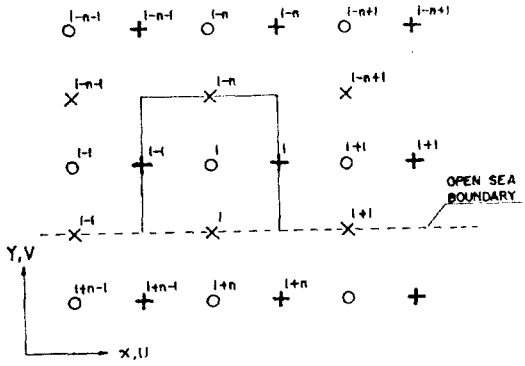


**Fig. 3.** Model elements adjacent to a southern open sea boundary

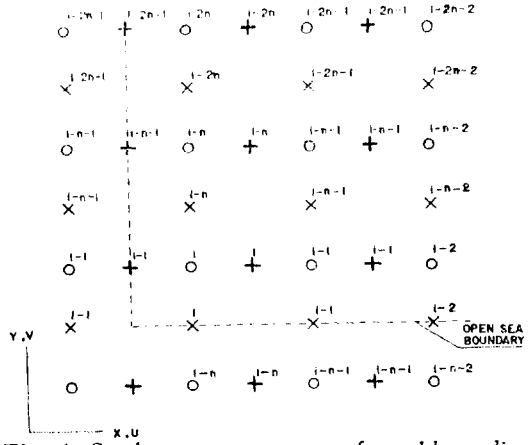


**Fig. 4.** Southwest convex corner formed by $x$-directed and $y$-directed open sea boundary

$$\begin{aligned}\frac{\{v_i(t+\Delta t)-v_i(t)\}}{\Delta t}=&-\frac{1}{4\Delta s}[\{u_i(t)+u_{i+n}(t)\}\{v_{i+1}(t)-v_i(t)\}\\&+\{u_{i-1}(t)+u_{i+n-1}(t)\}\{v_i(t+\Delta t)-v_{i-1}(t+\Delta t)\}]-\frac{1}{2\Delta s}\bar{v}_i(t)\{v_{i-n}(t+\Delta t)\\&-v_i(t+\Delta t)+v_i(t)-v_{i+n}(t)\}-fs_i(t+\Delta t)-\kappa\bar{v}_i(t+\Delta t)\{s_i^2(t)+v_i^2(t)\}^{\frac{1}{2}}/E_i(t)\\&-g\{\zeta_i(t+\Delta t)-\zeta_{i+n}(t+\Delta t)\}/\Delta s\end{aligned}\qquad(13)$$

where $\bar{u}_i=\frac{1}{4}(u_{i+1}+zu_i+u_{i-1})$,

$\bar{v}_i=\frac{1}{4}(v_{i-n}+zv_i+v_{i+n})$,

and similar equations for even timesteps with negative scan calculating $v$ first then $u$.

To allow for the drying of tidal flat area at low water, the following equations were used in conjunction with the above equations.

$u_i=0$ if $D_i<10$cm

$v_i=0$ if $E_i<10$cm

When elevation is specified as sea open boundary condition, $\zeta(t+\Delta t)=\hat{\zeta}(x,y,t+\Delta t)$ and $\zeta(t)=\hat{\zeta}(x,y,t)$ are prescribed at elevation points adjacent to the sea boundary, on that the equation of continuity (5) can be rearranged to give component of current across the boundary in terms of known quantities. For example, on a southern open boundary as in Fig. 3, equation (5) is re-written in the form

$$v_i(t)=\frac{1}{e_i(t)}\left[d_i(t)u_i(t)-d_{i-1}(t)u_{i-1}(t)+e_{i-n}(t)v_{i-n}(t)+\frac{\Delta s}{\Delta t}\left\{\zeta_i(t+\Delta t)-\zeta_i(t)\right\}\right]\qquad(14)$$

assuming $d_i(t)=\frac{1}{2}(h_i+\zeta_i+h_{i+1}+\zeta_i)$.

At a convex corner of an open boundary, as in Fig. 4, two currents across the boundary $u_{i-1}(t)$ and $v_i(t)$ are to be determined.

The flux across the open boundary into the corner element is $Q$,
where

$$\begin{aligned}Q(t)&=d_{i-1}(t)u_{i-1}(t)+e_i(t)v_i(t)\\&=d_i(t)u_i(t)+e_{i-n}(t)v_{i-n}(t)\\&\quad+\frac{\Delta s}{\Delta t}\left\{\zeta_i(t+\Delta t)-\zeta_i(t)\right\},\end{aligned}\qquad(15)$$

from continuity. The right hand side of this equation contains known quantities only. Initial estimates $u_{i-1}^{(0)}$, $v_i^{(0)}$ were provided by

$$\begin{aligned}u_{i-1}^{(0)}=&-4u_{i-n}+2(u_i+u_{i-n+1}+u_{i-2n}+u_{i-n-i})\\&-(u_{i+1}-u_{i-2n+1}+u_{i-2n-1}),\end{aligned}\qquad(16)$$

$$\begin{aligned}v_i^{(0)}=&-4v_{i-n+1}+2(v_{i+1}+v_{i-n+2}+v_{i-2n+1}+v_{i-n})\\&-(v_{i+2}+v_{i-2n+2}+v_{i-2n}),\end{aligned}\qquad(17)$$

Then assuming

$d_{i-1}=\frac{1}{2}(h_{i-1}+\zeta_i+h_i+\zeta_i)$,

and $e_i=\frac{1}{2}(h_i+\zeta_i+h_{i+n}+\zeta_i)$,

$v_i^{(1)}=\{Q-d_{i-1}u_{i-1}^{(0)}\}/e_i$,

$v_i^{(2)}=\frac{1}{2}\{v_i^{(0)}+v_i^{(1)}\}$,

$u_{i-1}^{(1)}=\{Q-e_iv_i^{(2)}\}/d_{i-1}$,

$u_{i-1}=\frac{1}{2}\{u_{i-1}^{(0)}+u_{i-1}^{(1)}\}$,

$v_i=\{Q-d_{i-1}u_{i-1}\}/e_i$,

so that the final estimates

$u_{i-1}=u_{i-1}(t)$ and $v_i=v_i(t)$ satisfy the equation of continuity(15).

## 3. Stability condition

Following Flather(1972), the stability criterion of a lincarised version of the scheme in Cartesian coordinates has a sufficient condition as

$$\Delta t<\{(1-\frac{1}{2}|f|\Delta t)/2gh\}^{\frac{1}{2}}\Delta s, \tag{18}$$

where $f=2\omega\sin\phi$, the coriolis parameter and $\Delta s$ is the grid spacing.

Flather concluded that equation(18) approximates closely the standard Courant-Friedrichs-Lewy criterion (Richtmyer and Morton, 1976) when in addition $f=0$.

$$\Delta t<\sqrt{\frac{2}{gh}}\left(\frac{\Delta s}{2}\right), \tag{19}$$

Taking the above criteria as a guide to the maximum time increment for stable difference solutions, and substituting

$\Delta s=1,853$m, $g=9.81$ms$^{-2}$ $h_{max}=60$m yields

$\Delta t=54$sec.

Accordingly the timestep chosen for the model was $\Delta t=1/72$ lunar hour.

Also it was decided to omit the advective terms within some grid distance of open sea boundaries since not all the values of current needed to solve equations (12) and (13) are available at $u, v$ points adjacent to open sea boundaries. For the present study, advective terms were omitted within a distance of $6\Delta s$ of these boundaries for the model to avoid instability orginated from the southwest corner of boundary.

## 4. Model grid and numerical data

The finite difference grid used in the model of Inchon Bay is shown in Fig. 1. The rectangular array comprising elements with $l=77$, $m=60$, for the model was introduced. Depths used for each model were taken from Korean hydrographic charts Nos. 306, 309 and 426. Chart depths were corrected to depths below mean sea level by adding the sum of the average amplitude of the $M_2$ and $S_2$ constituents taken over the surrounding area. Though large areas of shallow water were included and treated as drying banks within the model, the numerous channels and complex topography of drying banks are not resolvable by the present mesh dimensions. Accordingly the Han river and Yom Ha estuary were not identified in the present model.

Values of other parameters were taken as follow:

$f=8.87\times10^{-5}$s$^{-1}$,

$H_0=100$cm, $\kappa=0.0025\sim0.0045$

## 5. Computation of the $M_2$ tide

A series of numerical experiments were carried out to simulate the $M_2$ tidal distribution. Input at elevation points on the open western and southern boundary was specified as

$$\zeta(t)=H\cos(\sigma t-g), \tag{20}$$
$$=\zeta_1\cos\sigma t+\zeta_2\sin\sigma t$$

where $H$ is the amplitude and $g$ the phase of constituent with speed $\sigma$.

The speed of $M_2$ constituent is 30°/lunar hour and, for convenience, phase lag ($g$) was replaced by local phase lag ($\kappa$) referred to 135°E longitude. Amplitudes and phases specifying the open boundary conditions were obtained from the existing chart(Ogura, 1933) and results of harmonic analysis of coastal observations near the boundary. With timesteps chosen to satisfy

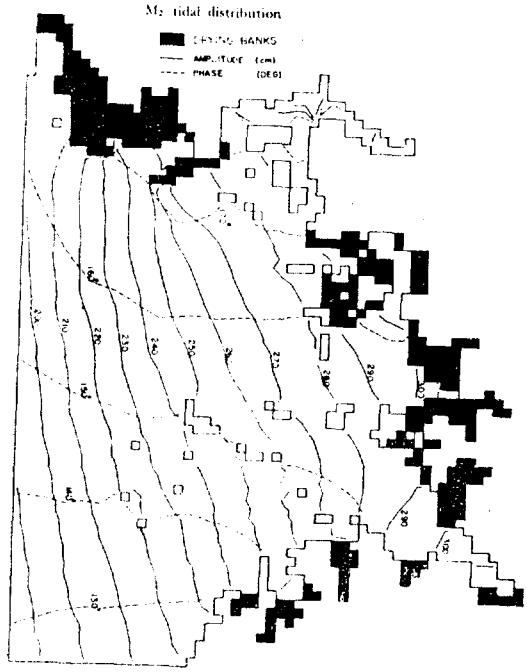

Fig. 5. Model generated $M_2$ tidal chart-Inchon Bay

the explicit stability conditions, the $M_2$ period is $864\Delta t$ which is convenient since the integer number of timesteps repeated for successive cycles.

A series of adjustments of friction parameter employing a depth varying relationship and amplitudes and phases of the $M_2$ tides at open boundary from the larger models covering the large sea area (Choi, 1980) and from the existing chart were made for the model to reproduce the tides observed at the coastal station correctly.

Finally the results were analysed for $M_2$ constituents by the Fourier analysis because the non-linearities in the governing equations of the system introduce integer multiples of fundamental frequency, i.e., $M_2$, $M_4$, $M_6$···. Data from the fourth cycle were taken for Fourier analysis since the motion had become essentially repeating.

## MODEL RESULTS

Assessment of the calculated $M_2$ tide has been investigated by comparison with the existing

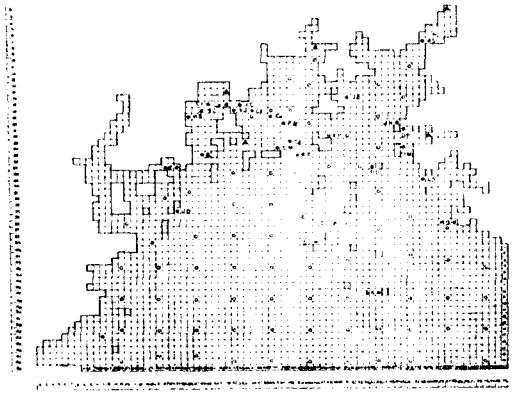

Fig. 6. Inchon Bay grid showing the location of elevation points( • ) from which computed results are compared with observed values at nearby station and points( ∘ ) at which the $M_2$ tidal current ellipses are presented and points( ▲ ) at which tidal profiles are presented

charts (Ogura, 1933) and by comparing amplitudes and phases of the observed and computed $M_2$ tide at selected coastal stations. The pattern of computed co-amplitude and co-tidal lines shown in Fig. 5 was in good agreement with that of the existing chart. It should be noted that existing chart is a theoretical construction based on a limited coastal data and therefore not necessarily represent the true condition.

For the comparison of computed results and observation, 19 coastal observation sites were selected. Table 1 shows the comparison of observed and calculated amplitude and phases of the $M_2$ tide for these sites. The location of model elevation points closest to the observation sites are shown in Fig. 6. Fig. 7 shows the calculated amplitude and phases of the $M_2$ tide were plotted against observed values, so the deviation from the line of unit gradient indicates the errors from computation. Typical error from the model are of order of $\pm$5cm in amplitude and $\pm5°$ in phase indicating remarkably good agreement.

The spatial distribution of depth-mean current and drying banks are shown at intervals cove-

**Table 1.** Comparison of observed and calculated amplitude $H(m)$ and phase $\kappa$(degree referred to 135°E) for the $M_2$ tide

| Station | Code | Position of Station | Observed | | Calculated | |
|---|---|---|---|---|---|---|
| | | | $H$ | $\kappa$ | $H$ | $\kappa$ |
| Duckjuckdo | DJ | 37°15′N 126°09′E | 2.48 | 140 | 2.52 | 145 |
| Jumundo | JD | 37°39′N 126°14′E | 2.70 | 157 | 2.73 | 158 |
| Soyado | SD | 37°14′N 126°10′E | 2.51 | 142 | 2.51 | 144 |
| Baegado | BA | 37°04′N 125°57′E | 2.20 | 132 | 2.20 | 133 |
| Naeri | NR | 37°38′N 126°23′E | 2.80 | 159 | 2.85 | 161 |
| Hwangsando | HS | 37°37′N 126°33′E | 2.97 | 155 | 3.06 | 158 |
| Seodo | SO | 37°34′N 126°24′E | 2.93 | 154 | 3.05 | 158 |
| Youngjongdo | YJ | 37°30′N 126°34′E | 2.93 | 151 | 3.00 | 152 |
| Inchon | IC | 37°29′N 126°37′E | 2.93 | 148 | 2.99 | 151 |
| Palmido | PM | 37°21′N 126°32′E | 2.84 | 144 | 2.87 | 148 |
| Youngheungdo | YH | 37°15′N 126°30′E | 2.78 | 141 | 2.80 | 145 |
| Somoouido | SM | 37°22′N 126°27′E | 2.77 | 141 | 2.83 | 148 |
| Pungdo | PD | 37°06′N 126°22′E | 2.59 | 137 | 2.65 | 135 |
| Umoodo | UM | 37°02′N 126°27′E | 2.62 | 136 | 2.64 | 139 |
| Asan | AS | 36°58′N 126°47′E | 3.03 | 144 | 3.04 | 145 |
| Janggohang | JH | 37°02′N 126°34′E | 2.83 | 143 | 2.83 | 140 |
| Hagampo | HG | 36°53′N 126°12′E | 2.29 | 126 | 2.33 | 122 |
| Dugampo | DP | 36°58′N 126°31′E | 2.69 | 138 | 2.74 | 139 |
| Garolim | GR | 36°57′N 126°19′E | 2.40 | 135 | 2.54 | 131 |

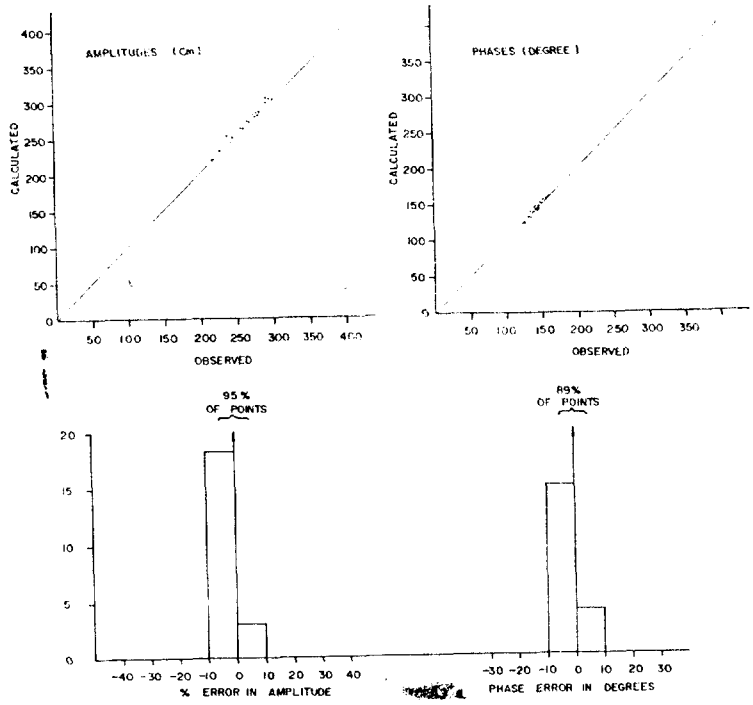


**Fig. 7.** Comparison between amplitudes and phases of the $M_2$ tide computed from the Inchon Bay model and observed value.

ring one tidal period in Fig. 8. The time of each plot is given in lunar hours after transit of Moon across 135°E meridian. In these figures, drying grid elements within the model are shaded and current vectors with small crosses at their origin are drawn representing the current obtained by averaging values at adjacent flow points. It is seen that the successive submergence of dry banks as the flood proceeds (hours 0~4) and the exposure of these areas

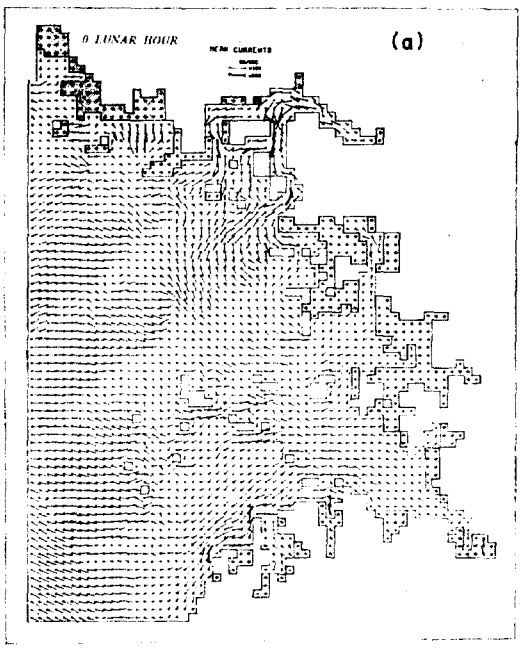


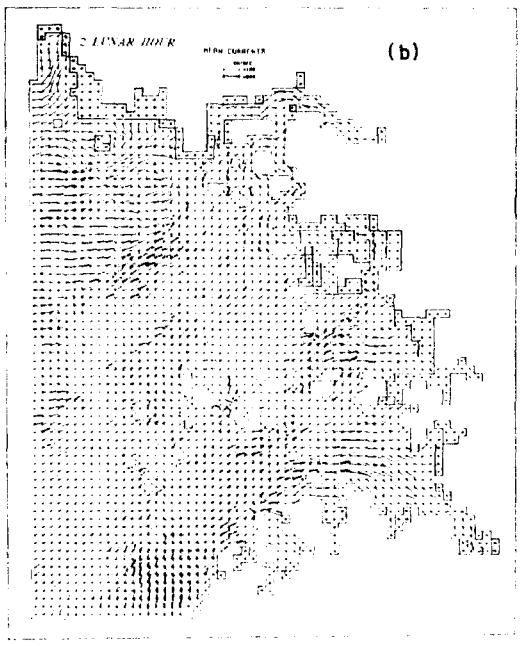


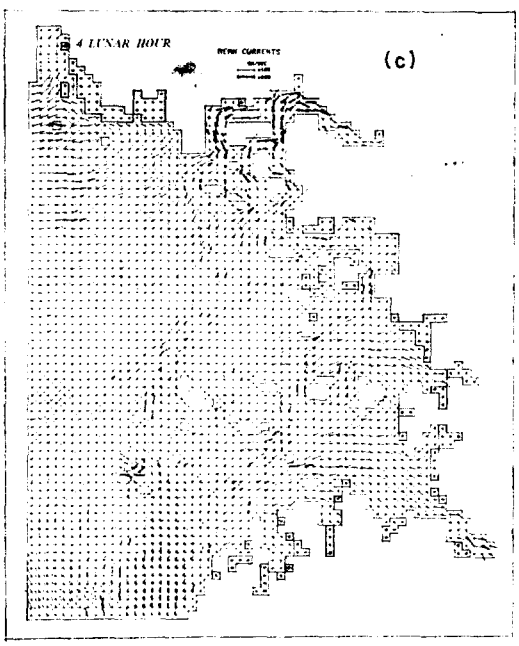


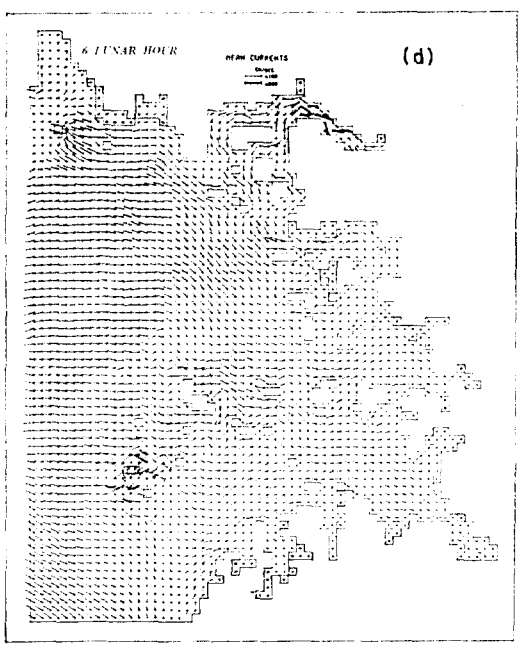

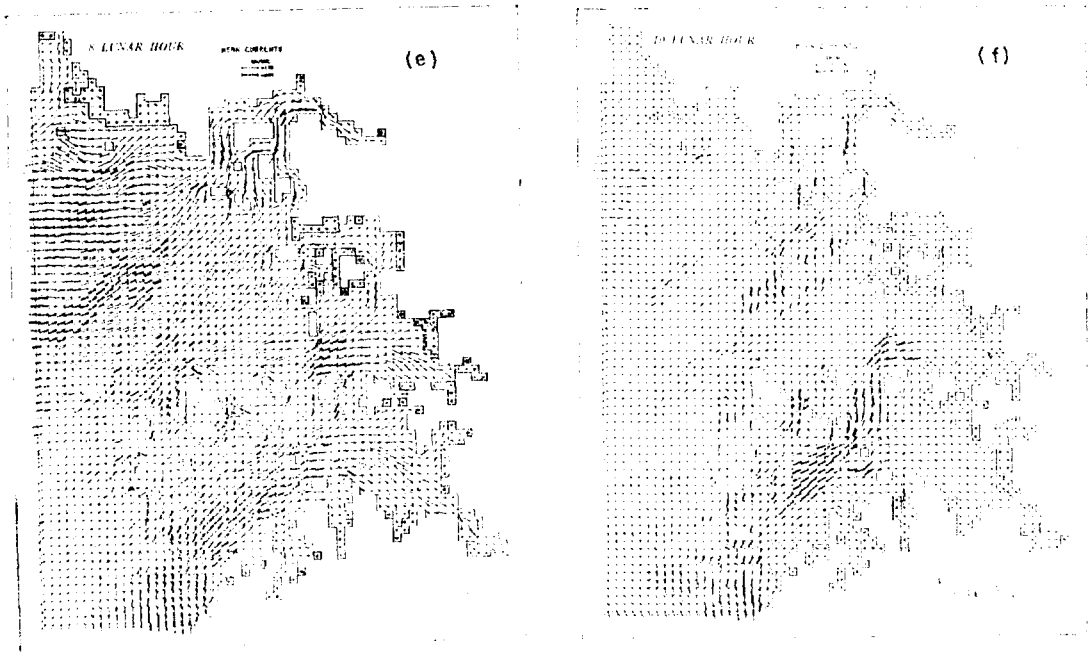


**Fig. 8(a)~(f).** The spatial distribution of depth-mean current and dry banks computed at intervals of two lunar hours.

with the ebb (hours 6~10) is sequentially represented. Sets of current vector also undergo harmonic oscillation of the same period, thus the Fourier analysis are performed on sets of values of east-going and north-going component of current for the last cycle and depth-mean $M_2$ tidal current ellipses are obtained (Fig. 9) for selected points. The ellipse chart gives magnitude and direction of the $M_2$ tidal current distribution representing the maximum and minimum velocity as major and minor axes respectively and magnitude and sense of rotation from 0 lunar hour are also indicated as arrows. It is seen that the $M_2$ tidal currents in the study region rotate anticlockwise through the tidal cycle and the elongated ellipses indicate a predominantly reversible current. Table 2 shows the comparison between computed current and observed values and appears to be good agreement.

The performance of the model in simulating the spatial distribution of drying area through

**Table 2.** Comparison between observed and calculated $M_2$ current ellipse

| Grid Point | Observed | | | Calculated | | |
|---|---|---|---|---|---|---|
| | major axes(cm) | minor axes(cm) | inclination from North (deg) | major axes(cm) | minor axes(cm) | inclination from North (deg) |
| $C_7$(29, 17) | 85 | 1 | 222 | 102 | 2 | 215 |
| $C_6$(32, 17) | 96 | 1 | 170 | 92 | 5 | 175 |
| $C_5$(36, 18) | 86 | 1 | 176 | 68 | 5 | 156 |
| $C_4$(39, 19) | 78 | 3 | 145 | 64 | 1 | 128 |
| $C_2$(42, 23) | 98 | 2 | 125 | 80 | 8 | 124 |
| B(28, 25) | 100 | 1 | 90 | 83 | 1 | 93 |
| $C_8$(44, 25) | 87 | 2 | 136 | 74 | 7 | 137 |

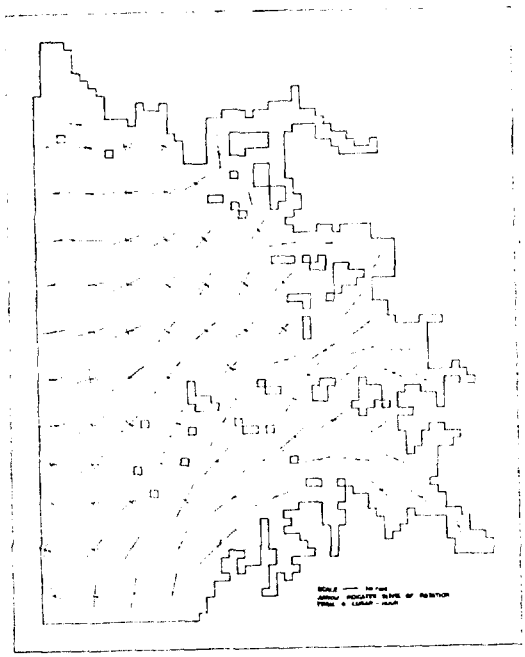

**Fig. 9.** The calculated $M_2$ tidal current ellipses at selected points in Inchon Bay.

a tidal cycle is already shown in Fig. 8. In Fig. 10, the sea surface, $\xi$, magnitude of the tidal current, $R$, and direction of the current, $\theta$, measured clockwise from the North of selected drying points, are plotted against time in lunar hours. Distortion at point (32, 15) in Kimpo area is such that the flood lasts for 3 lunar hours and the ebb for 3 lunar hours. Actual measurements on drying banks are necess-

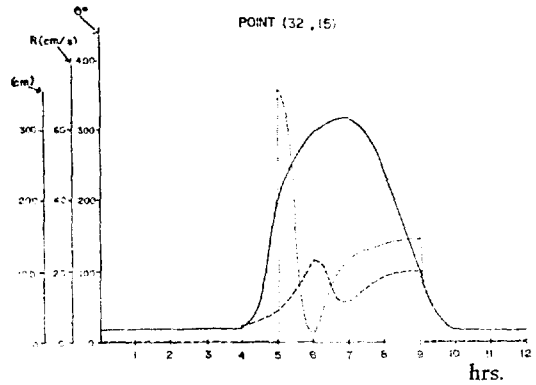


**Fig. 10.** Tidal profiles for 5 selected points in drying banks. (— ; elevation, ···depth-mean current, —·—·— direction of current measured clockwise from the north)

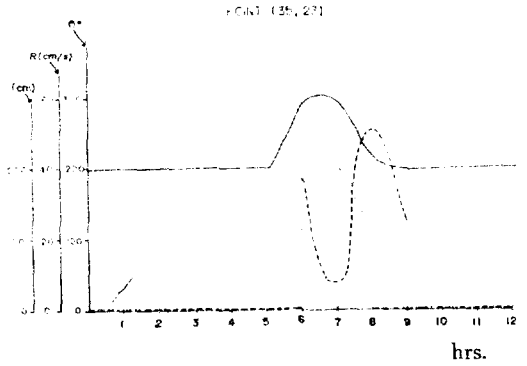


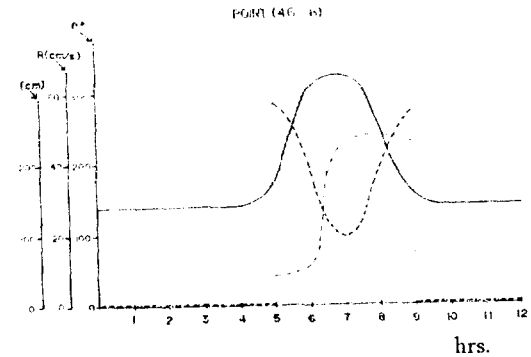


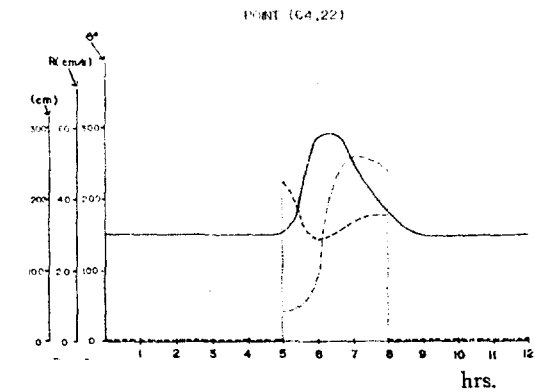


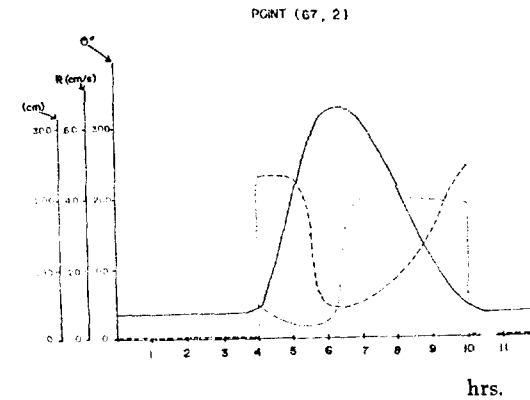

ary to investigate detailed flow behaviour in this area.

## CONCLUDING REMARKS

A numerical finite difference technique for tidal computations in shallow and shoaling water following Flather and Heaps (1975) was introduced and used to calculate the $M_2$ tide in Inchon Bay.

It is seen that the model reproduce adequately the drying boundary in Inchon Bay with the scheme employed. Comparisons between calculated and observed $M_2$ constants show that errors are typically $\pm$5cm in amplitude and $\pm5°$ in phase.

A furthur development of the model should include the improvement of open boundary values from sea measurement, a refinement of the grid to resolve the coastline more adequately, and the introduction of more tidal constituents.

## ACKNOWLEDGEMENTS

I am grateful to Dr. D.E. Cartwright for opportunity to study at IOS Bidston, U.K. and to Dr. H.S. Heaps for his kind supervision. The financial support provided by UNDP and British Council which sponsored this study are gratefully acknowledged.

## REFERENCES

Choi, B., 1978. Computation barrier effects on tides in Inchon Bay. Int. Symp. on Korea Tidal Power, KORDI, KIST, Nov. 14-15.

Choi, B., 1980. A tidal model of the Yellow Sea and the Eastern China Sea. KORDI Report 80-02.

Flather, R.A., 1972. Analytical and numerical studies in the theory of tides and storm surges. Ph.D. thesis, University of Liverpool.

Flather, R.A. and N.S. Heaps, 1975. Tidal computations for Morecambe Bay. Geophysical Journal of the Royal Astronomical Society, **42**:489-517.

Heaps, N.S., 1972. Tidal effects due to water generation in the Bristol Channel. pp. 435-455 in Tidal Power, (ed. T.J. Gray and O.K. Gashus). New York: Plenum Press. p. 630.

Heaps, N.S. and D.A. Greenberg, 1974. Mathematical model studies of tidal behaviour in the Bay of Fundy. Proc. IEEE International Conference on Engineering in the Ocean Environment. **1**:388-389. New York: Institute of Electrical and Electronic Engineers.

Leendertse, J.J. and E.C. Gritton, 1971. A water quality simulation model for well mixed estuaries and coastal seas: Vol. II, Computation procedures, Rand Corporation, R-708-NYC.

Ogura, S., 1933. The tides in the seas adjacent to Japan. Bulletin of the Hydrographic Department, Imperial Japanese Navy, 7.

Ramming, H.G., 1972. Reproduction of physical processes in coastal areas. Proc. 13th Conference on Coastal Engineering, Vancouver, ASCE.

Reid, R.O. and B.R. Bodine, 1968. Numerical model for storm surges in Galveston Bay. Journal of the Hydraulics Division, Proc. Am. Soc. Civ. Engrs., **94**:33-57.

Richtmyer, T.D. and K.W. Morton, 1967. Difference methods for initial value problems (2nd ed). New York: John Wiley.

Sielecki, A. and M.G. Wurtele, 1970. Convective difference schemes. Mathematics of Computation, **20**:272-299.